Arabian Journal of Chemistry 16 (2023) 105245

Contents lists available at ScienceDirect

Arabian Journal of Chemistry

journal homepage: www.sciencedirect.com

Original article

Pogocablanols A–G, a new class of sesquiterpenoids with an unprecedented bicyclic sesquiterpenoid skeleton from *Pogostemon cablin* (patchouli) and their activities

Qin-Mei Zhou [a,b,c,d,1], Huan Zhu [a,b,c,1], Chuan Ma [a,b], Li Guo [a,b], Cheng Peng [a,b,*], Liang Xiong [a,b,c,*]

[a] State Key Laboratory of Southwestern Chinese Medicine Resources, Chengdu University of Traditional Chinese Medicine, Chengdu 611137, China
[b] School of Pharmacy, Chengdu University of Traditional Chinese Medicine, Chengdu 611137, China
[c] Institute of Innovative Medicine Ingredients of Southwest Specialty Medicinal Materials, Chengdu University of Traditional Chinese Medicine, Chengdu 611137, China
[d] Innovative Institute of Chinese Medicine and Pharmacy, Chengdu University of Traditional Chinese Medicine, Chengdu 611137, China

ARTICLE INFO

Article history:
Received 9 March 2023
Accepted 4 September 2023
Available online 6 September 2023

Keywords:
Pogostemon cablin
Sesquiterpenoid
Pogocablane-type
Spirocyclic
Jejunum smooth muscle

ABSTRACT

Pogocablanols A–G (**1**–**7**), seven new compounds with an unprecedented sesquiterpenoid skeleton, were isolated from the aerial parts of *Pogostemon cablin*. This novel type of sesquiterpenoids, named pogocablane-type sesquiterpenoids, possesses a bicyclic nonisoprenoid system, including a five-membered carbocycle with a methyl group, a six-membered carbocycle with two methyl groups, and a methylene connecting the two carbocycles. Particularly, three isomers have an interesting 1-oxaspiro [4,4]nonane moiety. Their structures and absolute configurations were determined using extensive spectroscopic evidence, single-crystal X-ray diffraction, and electronic circular dichroism calculations. Pogocablanols A–D (**1**–**4**) exhibited a concentration-dependent inhibitory effect on rat jejunum smooth muscle contraction induced by acetylcholine, with E_{max} values varying from 48.87 ± 4.01% to 69.02 ± 7.54%. Preliminary structure–activity relationship analysis suggested that the oxaspirocycle and the pyran ring in pogocablanols are important structural features for the relaxing effects on jejunum smooth muscle. This study offered crucial support for more investigation and development of *P. cablin* by showing that these pogocablane-type sesquiterpenoids had the potential to be applied in pharmaceutical and functional food formulations.

1. Introduction

Sesquiterpenoids are a class of highly diversified structures composed of three isoprene units with acyclic and mono-, di-, tri-, and other-cyclic skeletons (Frage, 2013). They are a group of secondary metabolites that are widely distributed in plants, insects, and marine organisms (García-Davis et al., 2018; Tao et al., 2016). Generally, sesquiterpenoids have complex chemical structures and a broad spectrum of biological properties, such as antitumor, anti-inflammatory, and antibacterial activities (Chen et al., 2011; Wang et al., 2012; Jiang et al., 2021). Many sesquiterpenoids have been employed as ideal candidates for lead structures in drug discovery or tool compounds in biomedical studies (Chen et al., 2019). However, these molecules contain various skeletons and multiple stereogenic centers, which make absolute configuration determination a daunting task.

Pogostemon cablin (Blanco) Benth. (patchouli), a member of the Lamiaceae family, has been used to regulate gastrointestinal functions and treat colds, nausea, fever, headache, and diarrhea in China (Xu et al., 2022; Chen et al., 2013). Numerous Chinese patent medicines contain *P. cablin* as a raw material, such as Huoxiang Zhengqi Oral Liquid and Baoji Pill, which are effective at treating gastrointestinal disorders and are well known in China (Liu et al., 2014; Zhao et al., 2019; Chen et al., 2021). A growing body of evidence has revealed that patchouli and its extracts exert various pharmacological effects, such as anti-inflammatory, antipathogenic, antioxidative, and vasodilatory effects (Chen et al., 2021; Swamy and Sinniah, 2015; Galovičová et al., 2022; Hu et al.,

* Corresponding authors.
E-mail addresses: pengcheng@cdutcm.edu.cn (C. Peng), xiling@cdutcm.edu.cn (L. Xiong).
[1] Both authors contributed equally to this work.

Peer review under responsibility of King Saud University.

Production and hosting by Elsevier

https://doi.org/10.1016/j.arabjc.2023.105245
1878-5352/

2018). Patchouli oil is also commonly used in perfumery and aromatherapy and has tremendous business potential in the global market. Phytochemical studies have demonstrated that sesquiterpenoids are representative constituents of patchouli oil, including patchoulol-, patchoulene-, and guaiane-type sesquiterpenes (Xu et al., 2022). Our previous studies of patchouli oil led to the isolation of several sesquiterpenoids. (Zhou et al., 2018a, 2022; Zhu et al., 2017).

In the present study, seven bicyclic sesquiterpenoids (pogocablanols A–G, **1**–**7**) featuring a nonisoprenoid system with a C5-C1-C6 carbon skeleton were obtained (Fig. 1), and this new type of sesquiterpenoids was named pogocablane-type sesquiterpenoids. Pogocablanols A–C (**1**–**3**) are isomers possessing an interesting 1-oxaspiro[4,4]nonane moiety; pogocablanol D (**4**) has a 1-O-8 linkage to form a pyran ring fused with the five- and six-membered carbocycles; and pogocablanols F and G (**6** and **7**) are epimers. Of these isolates, compounds **1**–**4** act as relaxants on isolated rat jejunum strips pre-treated with acetylcholine (Ach). Compound **2** exhibited a moderate inhibitory effect against foam cell formation in RAW264.7 macrophages induced by oxidized low-density lipoprotein (ox-LDL). Herein, we describe the isolation, structural elucidation, plausible biosynthetic pathway, and biological evaluation of compounds **1**–**7**.

2. Materials and methods

2.1. General experimental procedures

Optical rotations were measured on a Rudolph Autopol-I automatic polarimeter (Rudolph Research Analytical, USA). UV and CD spectra were recorded using an Applied Photophysics Chirascan and Chirascan-plus circular dichroism spectrometer (Applied Photophysics Ltd., Leatherhead, England). An Agilent Cary 600 FT-IR microscope instrument (Agilent Technologies Inc., CA, USA) was used to measure IR spectra. NMR data were obtained by a Bruker-AVIIIHD-600 spectrometer (Bruker Corporation, MA, USA) with the solvent peaks used as references. HR-ESI-MS data were acquired on a Waters Synapt G_2 HDMS instrument (Waters Corporation Milford, MA, USA). X-ray crystallographic analysis was performed on a Bruker D8 Quest diffractometer with Cu Kα radiation. Column chromatography was performed using silica gel (200–300 mesh; Yantai Institute of Chemical Technology, Yantai, China), and Toyopearl HW-40F (Tosoh Corp., Japan). TLC was performed using glass precoated silica gel GF_{254} plates (Qingdao Marine Chemical Inc., Shandong, China). MPLC separations were performed using a BÜCHI Gradient Former B-687 instrument (BÜCHI, Flawil, Switzerland). HPLC separation was carried out using an Agilent 1100 instrument with a Kromasil semi-preparative C_{18} column (250×10 mm^2, 5 μm) for reversed-phase semi-preparative HPLC. Fetal bovine serum (FBS) was purchased from Zhejiang Tianhang Biotechnology Co., Ltd, and dulbecco's modified Eagle's medium (DMEM) was purchased from Hyclone (Logan, UT, USA). Assays for relaxant activity were conducted with a Radnoti 8 Channel Tissue Bath System (Radnoti Glass Tech., Monrovia, CA).

2.2. Plant material

Pogostemon cablin (Blanco) Benth. was collected in Yangchun City, Guangdong Province, China, in December 2012. The sample was identified by Dr. Fei Long and deposited in the School of Pharmacy in Chengdu University of TCM, Chengdu, China (voucher specimen: SGHX-20121224).

2.3. Extraction and isolation

The air-dried leaves and stems of *P. cablin* (40 kg) were subjected to hydrodistillation for 10 h using a big modified Clevenger-type apparatus with a water-cooled oil receiver to obtain the essential oil (215 g). After dried with anhydrous sodium sulfate, the oil was subjected to silica gel column chromatography using a gradient elution of increasing EtOAc (0–100%) in petroleum ether to give 31 fractions (F_1–F_{31}) on the basis of TLC analysis. F_{18} (15.5 g) was further separated by reversed-phase (RP) MPLC with a gradient of increasing MeOH (40–100%) in water to afford 14 subfractions ($F_{18\text{-}1}$–$F_{18\text{-}14}$). The subfraction $F_{18\text{-}2}$ was isolated via silica gel column chromatography with a gradient solvent system (100:1–5:1, $CHCl_3$–Me_2CO) to obtain 11 subfractions ($F_{18\text{-}2\text{-}1}$–$F_{18\text{-}2\text{-}11}$). Further purification of $F_{18\text{-}2\text{-}3}$ by preparative TLC (CH_2Cl_2–*n*-hexane–Me_2CO, 3:1:0.1) and semipreparative RP HPLC (45% MeOH in H_2O) successively afforded compounds **2** (4.6 mg, t_R = 45 min) and **3** (3.5 mg, t_R = 56 min). The subfraction $F_{18\text{-}2\text{-}6}$ was purified via preparative TLC (CH_2Cl_2–*n*-hexane–Me_2CO, 2:1:0.1) to obtain compound **1** (5.6 mg). The subfraction $F_{18\text{-}2\text{-}7}$ was further divided into four parts ($F_{18\text{-}2\text{-}7\text{-}1}$–$F_{18\text{-}2\text{-}7\text{-}4}$) using a Toyopearl HW-40F column (85% MeOH in H_2O, v/v). $F_{18\text{-}2\text{-}7\text{-}2}$ was applied to preparative TLC (CH_2Cl_2–*n*-hexane–Me_2CO, 4:1:0.1) to yield compound **5** (4.7 mg). $F_{18\text{-}2\text{-}7\text{-}3}$ was further separated by semipreparative RP HPLC (50% MeOH in H_2O) to yield compound **6** (6.3 mg, t_R = 42 min). Compounds **4** (5.1 mg) and **7** (6.2 mg) were obtained from $F_{18\text{-}2\text{-}8}$ via preparative TLC (CH_2Cl_2–*n*-hexane–Me_2CO, 2:1:0.1).

2.3.1. Pogocablanol A (*1*)

Colorless crystals (MeOH); $[\alpha]_D^{20}$ −7.5 (*c* 0.04, MeOH); UV (MeCN) λ_{max} (log ε) 279 (2.55) nm; ECD (MeCN) λ_{max} ($\Delta\varepsilon$) 201 (−1.6), 319 (−0.1) nm; IR (KBr) ν_{max} 3445, 2950, 2885, 1737, 1600, 1457, 1382,

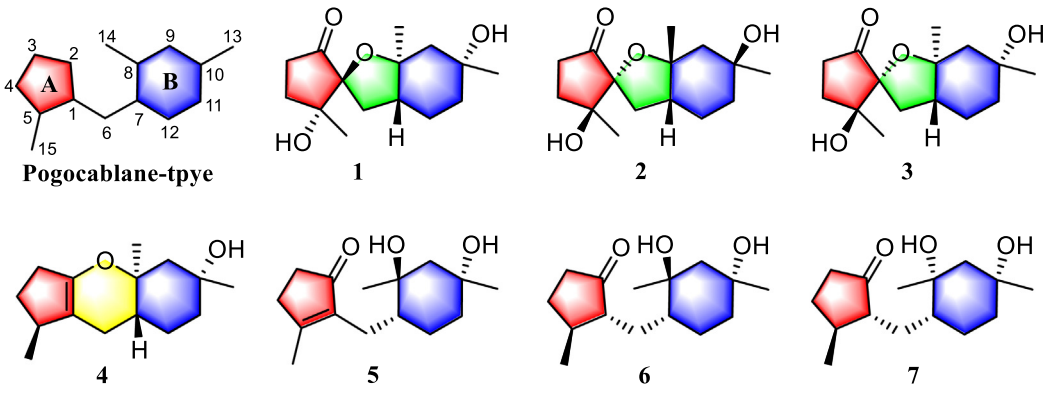

Fig. 1. Structure of compounds **1**–**7**.

Table 1
^{1}H NMR (600 MHz) Data of Compounds **1**–**7** in Acetone d_6 (δ in ppm, J in Hz).

no.	1	2	3	4	5	6	7
1						1.72 m	1.67 m
3	2.25 ddd (18.6, 10.2, 3.0)	2.23 ddd (18.6, 9.6, 7.2)	2.24 ddd (16.2, 9.6, 6.6)	2.20 m	2.25 m	2.21 m	2.20 m
	2.17 dt (18.6, 9.0)	2.16 ddd (18.6, 9.6, 5.4)	2.15 ddd (16.2, 9.6, 6.6)	2.09 m		2.08 m	2.10 dd (15.6, 9.0)
4	2.00 dd (12.0, 10.2, 9.0)	1.92 ddd (12.6, 9.6, 7.2)	1.94 ddd (15.6, 9.6, 6.6)	2.03 m	2.51 m	2.10 m	2.07 m
	1.81 ddd (12.0, 9.0, 3.0)	1.86 ddd (12.6, 9.6, 5.4)	1.87 ddd (15.6, 9.6, 6.0)	1.25 m		1.41 m	1.42 m
5				2.57 m		1.85 m	1.79 m
6	1.97 dd (12.6, 5.4)	2.21 t (12.6)	2.02 dd (13.2, 12.0)	1.87 dd (13.2, 3.0)	2.58 d (13.2)	1.94 ddd (13.8, 9.0, 3.0)	1.75 m
	1.94 t (12.6)	1.66 dd (12.6, 6.6)	1.70 dd (12.0, 6.0)	1.51 overlapped	1.92 dd (13.2, 10.2)	1.16 m	1.31 ddd (13.8, 10.2, 3.0)
7	1.67 m	2.36 m	1.90 m	1.48 m	1.39 m	1.62 m	1.60 m
9	1.91 dd (12.6, 1.8)	1.68 d (14.4)	1.91 dd (12.6, 1.8)	1.88 d (13.8)	1.77 dd (13.2, 2.4)	1.76 dd (13.8, 2.4)	1.65 d (14.4)
	1.51 d (12.6)	1.59 overlapped	1.51 d (12.6)	1.52 overlapped	1.47 d (13.2)	1.48 d (13.8)	1.44 d (14.4)
11	1.77 m	1.51 m	1.76 m	1.66 m	1.53 m	1.58 m	1.65 m
	1.44 m	1.38 m	1.44 m	1.43 m	1.19 m	1.32 m	1.36 m
12	1.64 m	2.00 m	1.59 m	1.50 m	1.37 m	1.49 m	1.51 m
	1.48 m	1.56 m	1.47 m	1.47 m	1.28 m	1.35 m	1.51 m
13	1.22 s	1.16 s	1.26 s	1.21 s	1.14 s	1.16 s	1.13 s
14	1.19 d (1.2)	1.36 d (1.2)	1.29 d (1.2)	1.20 s	1.27 brs	1.20 brs	1.13 s
15	1.27 s	1.25 s	1.21 s	0.97 d (6.6)	2.07 s	1.13 d (6.6)	1.13 d (6.0)
OH-5	3.81 s	3.82 s	3.83 s				
OH-8					3.11 s	2.94 s	4.28 s
OH-10	3.12 s	2.98 s	3.11 s	3.14 s	2.92 s	2.92 s	4.23 s

1313, 1273, 1143, 1090, 1036, 981, 916, 855, 747, 561 cm^{-1}; ^{1}H NMR (acetone d_6, 600 MHz) and ^{13}C NMR (acetone d_6, 150 MHz) data, see Tables 1 and 2, respectively. HR-ESI-MS m/z 291.1574 [M + Na]$^+$ (calcd. for $C_{15}H_{24}O_4Na$, 291.1572).

2.3.2. Pogocablanol B (**2**)

Colorless crystals (MeOH); $[\alpha]_D^{20}$ + 4.3 (c 0.07, MeOH); UV (MeCN) λ_{max} (log ε) 279 (2.48) nm; ECD (MeCN) λ_{max} ($\Delta\varepsilon$) 207 (+0.8), 310 (−0.2) nm; IR (KBr) ν_{max} 3480, 3305, 2967, 2934, 1748, 1643, 1455, 1380, 1266, 1202, 1131, 1064, 967, 903, 844, 761, 572 cm^{-1}; ^{1}H NMR (acetone d_6, 600 MHz) and ^{13}C NMR (acetone d_6, 150 MHz) data, see Tables 1 and 2, respectively. HR-ESI-MS m/z 291.1572 [M + Na]$^+$ (calcd. for $C_{15}H_{24}O_4Na$, 291.1572).

2.3.3. Pogocablanol C (**3**)

Colorless crystals (MeOH); $[\alpha]_D^{20}$ + 1.9 (c 0.05, MeOH); UV (MeCN) λ_{max} (log ε) 279 (2.36) nm; ECD (MeCN) λ_{max} ($\Delta\varepsilon$) 206 (+1.2), 310 (−0.4) nm; IR (KBr) ν_{max} 3454, 2937, 1745, 1643, 1458, 1377, 1197, 1152, 1087, 1029, 980, 893, 845, 746, 653, 612, 559 cm^{-1}; ^{1}H NMR (acetone d_6, 600 MHz) and ^{13}C NMR (acetone d_6, 150 MHz) data, see Tables 1 and 2, respectively. HR-ESI-MS m/z 291.1576 [M + Na]$^+$ (calcd. for $C_{15}H_{24}O_4Na$, 291.1572).

Table 2
^{13}C NMR (150 MHz) Data of Compounds **1**–**7** in Acetone d_6 (δ in ppm).

no.	1	2	3	4	5	6	7
1	88.9	89.7	90.7	111.0	140.9	55.1	54.4
2	216.0	216.8	216.2	149.7	209.1	220.9	220.5
3	33.1	32.7	32.7	31.3	34.8	38.3	38.3
4	33.8	34.2	34.1	30.4	32.0	30.2	30.3
5	77.7	76.9	77.0	38.9	170.9	38.4	38.9
6	27.8	31.1	30.3	25.2	23.3	28.5	28.9
7	50.2	42.9	48.2	41.9	48.9	46.2	43.6
8	84.7	84.2	84.2	78.9	72.8	72.9	73.0
9	52.0	48.7	52.1	51.5	54.7	54.9	51.0
10	71.5	70.0	71.5	70.9	70.9	70.8	71.4
11	41.8	33.3	41.8	40.2	39.9	39.9	39.8
12	23.6	21.6	23.1	27.1	26.1	26.5	24.2
13	33.9	32.8	33.9	33.1	32.9	32.9	31.6
14	20.8	29.1	22.6	18.4	23.4	23.4	29.0
15	22.2	22.6	23.3	20.8	17.5	19.7	19.6

2.3.4. Pogocablanol D (**4**)

Colorless crystals (MeOH); $[\alpha]_D^{20}$ −6.5 (c 0.06, MeOH); UV (MeCN) λ_{max} (log ε) 239 (3.18) nm; ECD (MeCN) λ_{max} ($\Delta\varepsilon$) 216 (+0.1) nm, 253 (−0.5), 339 (+0.1) nm; IR (KBr) ν_{max} 3430, 2932, 1702, 1634, 1516, 1455, 1383, 1258, 1140, 1093, 1035, 914, 848, 662, 579, 521 cm^{-1}; ^{1}H NMR (acetone d_6, 600 MHz) and ^{13}C NMR (acetone d_6, 150 MHz) data, see Tables 1 and 2, respectively. HR-ESI-MS m/z 259.1676 [M + Na]$^+$ (calcd. for $C_{15}H_{24}O_2Na$, 259.1674).

2.3.5. Pogocablanol E (**5**)

Colorless crystals (MeOH); $[\alpha]_D^{20}$ + 5.05 (c 0.03, MeOH); UV (MeCN) λ_{max} (log ε) 232 (3.50), 279 (2.49) nm; ECD (MeCN) λ_{max} ($\Delta\varepsilon$) 302 (−0.6) nm; IR (KBr) ν_{max} 3407, 2945, 1733, 1620, 1525, 1450, 1380, 1177, 1048, 969, 900, 842, 670 cm^{-1}; ^{1}H NMR (acetone d_6, 600 MHz) and ^{13}C NMR (acetone d_6, 150 MHz) data, see Tables 1 and 2, respectively. HR-ESI-MS m/z 275.1634 [M + Na]$^+$ (calcd. for $C_{15}H_{24}O_3Na$, 275.1623).

2.3.6. Pogocablanol F (**6**)

Colorless crystals (MeOH); $[\alpha]_D^{20}$ −5.56 (c 0.05, MeOH); UV (MeCN) λ_{max} (log ε) 279 (2.21) nm; ECD (MeCN) λ_{max} ($\Delta\varepsilon$) 300 (−1.0) nm; IR (KBr) ν_{max} 3309, 2967, 2932, 2874, 1724, 1615, 1460, 1368, 1317, 1159, 1085, 1032, 950, 917, 852, 774, 676, 483 cm^{-1}; ^{1}H NMR (acetone d_6, 600 MHz) and ^{13}C NMR (acetone d_6, 150 MHz) data, see Tables 1 and 2, respectively. HR-ESI-MS m/z 277.1784 [M + Na]$^+$ (calcd. for $C_{15}H_{26}O_3Na$, 277.1780).

2.3.7. Pogocablanol G (**7**)

Colorless crystals (MeOH); $[\alpha]_D^{20}$ −2.72 (c 0.10, MeOH); UV (MeCN) λ_{max} (log ε) 279 (2.51) nm; ECD (MeCN) λ_{max} ($\Delta\varepsilon$) 300 (−1.4) nm; IR (KBr) ν_{max} 3346, 2937, 2868, 1732, 1457, 1373, 1334,

1276, 1209, 1162, 1093, 1028, 960, 901, 843, 678, 578 cm^{-1}; ^1H NMR (acetone d_6, 600 MHz) and ^{13}C NMR (acetone d_6, 150 MHz) data, see Tables 1 and 2, respectively. HR-ESI-MS *m/z* 277.1779 $[M + Na]^+$ (calcd. for $C_{15}H_{26}O_3Na$, 277.1780).

2.4. X-ray crystallographic analysis

2.4.1. Crystal data for pogocablanol A (**1**)

$C_{15}H_{24}O_4$, *M* = 268.34, orthorhombic, $P2_12_12_1$, *a* = 8.5111(6) Å, *b* = 12.6780(9) Å, *c* = 13.2105(9) Å, α = 90.00°, β = 90.00°, γ = 90.00°, *V* = 1425.46(17) $Å^3$, *T* = 150(2) K, *Z* = 4, μ(Cu Kα) = 0.724 mm^{-1}, 7426 reflections measured, 2397 independent reflections (R_{int} = 0.0500). The final R_1 values were 0.0358 ($I > 2\sigma(I)$). The final $wR(F^2)$ values were 0.0905 ($I > 2\sigma(I)$). The final R_1 values were 0.0372 (all data). The final $wR(F^2)$ values were 0.0922 (all data). The goodness of fit on F^2 was 1.055. Flack parameter = −0.14(13). CCDC number: 2195623.

2.4.2. Crystal data for pogocablanol B (**2**)

$C_{15}H_{24}O_4{\cdot}H_2O$, *M* = 286.36, orthorhombic, $P2_12_12_1$, *a* = 10.7328(8) Å, *b* = 11.5772(9) Å, *c* = 12.1269(9) Å, α = 90.00°, β = 90.00°, γ = 90.00°, *V* = 1506.8(2) $Å^3$, *T* = 150(2) K, *Z* = 4, μ(Cu Kα) = 0.766 mm^{-1}, 12,516 reflections measured, 2740 independent reflections (R_{int} = 0.0651). The final R_1 values were 0.0393 ($I > 2\sigma(I)$). The final $wR(F^2)$ values were 0.1063 ($I > 2\sigma(I)$). The final R_1 values were 0.0417 (all data). The final $wR(F^2)$ values were 0.1079 (all data). The goodness of fit on F^2 was 0.954. Flack parameter = −0.01(12). CCDC number: 2195626.

2.4.3. Crystal data for pogocablanol C (**3**)

$C_{15}H_{24}O_4{\cdot}H_2O$, *M* = 286.36, monoclinic, $P2_1$, *a* = 7.9179(3) Å, *b* = 9.9075(4) Å, *c* = 18.9485(7) Å, α = 90.00°, β = 94.192(2)°, γ = 90.00°, *V* = 1482.47(10) $Å^3$, *T* = 150(2) K, *Z* = 4, μ(Cu Kα) = 0.779 mm^{-1}, 28,710 reflections measured, 5353 independent reflections (R_{int} = 0.0654). The final R_1 values were 0.0464 ($I > 2\sigma(I)$). The final $wR(F^2)$ values were 0.1215 ($I > 2\sigma(I)$). The final R_1 values were 0.0493 (all data). The final $wR(F^2)$ values were 0.1252 (all data). The goodness of fit on F^2 was 1.059. Flack parameter = 0.07(8). CCDC number: 2195628.

2.4.4. Crystal data for pogocablanol D (**4**)

$C_{15}H_{24}O_2$, *M* = 236.34, monoclinic, $P2_1$, *a* = 14.7874(6) Å, *b* = 6.6945(3) Å, *c* = 24.9964(10) Å, α = 90.00°, β = 90.127(2)°, γ = 90.00°, *V* = 2474.49(18) $Å^3$, *T* = 130(2) K, *Z* = 6, μ(Cu Kα) = 0.478 mm^{-1}, 40,679 reflections measured, 9752 independent reflections (R_{int} = 0.0474). The final R_1 values were 0.0348 ($I > 2\sigma(I)$). The final $wR(F^2)$ values were 0.0862 ($I > 2\sigma(I)$). The final R_1 values were 0.0394 (all data). The final $wR(F^2)$ values were 0.0886 (all data). The goodness of fit on F^2 was 1.069. Flack parameter = 0.01(7). CCDC number: 2195629.

2.4.5. Crystal data for pogocablanol E (**5**)

$C_{15}H_{24}O_3$, *M* = 252.34, trigonal, $P3_12_1$, *a* = 10.7354(3) Å, *b* = 10.7354(3) Å, *c* = 21.9546(5) Å, α = 90.00°, β = 90.00°, γ = 120.00°, *V* = 2191.25(13) $Å^3$, *T* = 295(2) K, *Z* = 6, μ(Cu Kα) = 0.623 mm^{-1}, 33,166 reflections measured, 2670 independent reflections (R_{int} = 0.0384). The final R_1 values were 0.0279 ($I > 2\sigma(I)$). The final $wR(F^2)$ values were 0.0788 ($I > 2\sigma(I)$). The final R_1 values were 0.0289 (all data). The final $wR(F^2)$ values were 0.0800 (all data). The goodness of fit on F^2 was 1.047. Flack parameter = −0.01(5). CCDC number: 2195627.

2.4.6. Crystal data for pogocablanol F (**6**)

$C_{15}H_{26}O_3{\cdot}H_2O$, *M* = 272.37, orthorhombic, $P2_12_12_1$, *a* = 7.7488(3) Å, *b* = 8.2000(3) Å, *c* = 24.0707(10) Å, α = 90.00°, β = 90.00°, γ = 90.00°, *V* = 1529.46(10) $Å^3$, *T* = 150(2) K, *Z* = 4, μ(Cu Kα) = 0.675 mm^{-1}, 14,061 reflections measured, 2803 independent reflections (R_{int} = 0.0520). The final R_1 values were 0.0327 ($I > 2\sigma(I)$). The final $wR(F^2)$ values were 0.0887 ($I > 2\sigma(I)$). The final R_1 values were 0.0333 (all data). The final $wR(F^2)$ values were 0.0893 (all data). The goodness of fit on F^2 was 1.016. Flack parameter = −0.07(7). CCDC number: 2195625.

2.4.7. Crystal data for pogocablanol G (**7**)

$C_{15}H_{26}O_3$, *M* = 254.36, orthorhombic, $P2_12_12_1$, *a* = 6.0265(2) Å, *b* = 8.9385(2) Å, *c* = 27.5773(6) Å, α = 90.00°, β = 90.00°, γ = 90.00°, *V* = 1485.53(7) $Å^3$, *T* = 273(2) K, *Z* = 4, μ(Cu Kα) = 0.613 mm^{-1}, 23,361 reflections measured, 2713 independent reflections (R_{int} = 0.0494). The final R_1 values were 0.0388 ($I > 2\sigma(I)$). The final $wR(F^2)$ values were 0.0981 ($I > 2\sigma(I)$). The final R_1 values were 0.0456 (all data). The final $wR(F^2)$ values were 0.1049 (all data). The goodness of fit on F^2 was 1.029. Flack parameter = 0.13(10). CCDC number: 2195624.

2.5. Effects of compounds **1**–**7** on acetylcholine-induced contractions of rat jejunum smooth muscle

Male Sprague-Dawley rats (200–220 g) were obtained from Da Shuo Biotechnology Co., Ltd (Chengdu, Sichuan, China). All rats were maintained on a 12 h light/dark cycle under a controlled temperature at 25 ± 1 °C and a relative humidity of 50 ± 5%. All the experimental procedures were performed in accordance with the guidelines of the Management Committee for Experimental Animals, China. Animals were fasted for 12 h but free access to water before used. The animal was sacrificed by cervical dislocation, and then the jejunum smooth muscle was carefully dissected and immediately transferred into oxygenated Tyrode's solution [composition (mM): NaCl, 136.9; KCl, 2.7; $NaHCO_3$, 11.9; NaH_2PO_4, 0.4; $MgCl_2$, 1.1; glucose, 5.6; $CaCl_2$, 1.8] at 4 °C (Ghayur et al., 2005). The jejunum was cleaned of surrounding fat and connective tissues and cut into approximately 1–2 cm in length, and then suspended in Tyrode's solution at a constant temperature of 37 °C and bubbled with a gas mixture of 95% O_2 and 5% CO_2. All the muscles were equilibrated under an initial tension of 1 g in normal Tyrode's solution before the start of the experiment (Bian et al., 2015). The jejunum smooth muscles were pre-contracted with 1 mg/mL acetylcholine (Ach) solution. When the muscles were stably contracted, the cumulative concentrations of the test compounds (0.5, 1.5, 5, 15, and 50 μM) and dimethyl sulfoxide (DMSO) were added into the organ bath, and the effects were recorded. The relaxation and E_{max} (maximal relaxation) values of the test compounds were calculated.

2.6. Effects of compounds **1**–**7** on ox-LDL-induced RAW264.7 macrophage foam cells formation

2.6.1. Cell culture

RAW264.7 cells were purchased from the Cell Bank of Shanghai Institute of Biological Sciences, Chinese Academy of Sciences (Shanghai, China). The cells were grown in DMEM medium supplemented with 10% FBS and 1% penicillin/streptomycin, and they were incubated in an incubator (Thermo Fisher Scientific, Marietta, USA) at 37 °C with a humidified atmosphere containing 5% CO_2. The cells were randomly divided into different groups.

2.6.2. Cell viability assay

The viability of RAW264.7 cells was measured by the CCK8 assay (Cao et al., 2019). When the cells reached 70–80% confluency, they were inoculated in 96-well plate (3×10^4 cells/well). After cell adherence, the different concentrations of compounds (12.5, 25, and 50 μM) were added for 24 h. Then, 10 μL CCK-8 solution was added per well, and the absorbance optical density (OD) at

450 nm wavelength was measured using an enzyme labeling instrument (Molecular devices, Shanghai, China) after 1 h.

2.6.3. Nile red staining

Lipid accumulation in RAW264.7 macrophages was measured by Nile red staining (Yuan et al., 2020). Cells were cultured on 24-well culture plates, and the cells treated with ox-LDL were used as the model group, whereas those treated with ox-LDL and different concentrations of compound **2** (12.5, 25, and 50 μM) were used as the drug groups. After a 24 h treatment, cells were fixed with 4% paraformaldehyde (Biosharp, Anhui, China) for 30 min and then incubated with 0.25 μg/mL Nile red (Biosharp, Anhui, China) for 30 min. Subsequently, the cells were cleaned with PBS for 3 times, and the lipid accumulation was characterized by the intensity detected at 530/590 nm (Molecular devices, Shanghai, China).

2.6.4. Oil red O staining

Cells were cultured on 24-well culture plates and treated with the same grouping, dose, and route of administration as Nile red staining. After a 24-h treatment, the cells were gently washed twice with PBS and fixed with 4% paraformaldehyde for 30 min. The cells were rinsed with 60% isopropanol for 30 s and stained by oil red O staining solution (Servicebio, Wuhan, China) for 30 min. The cells were cleaned with 50% isopropanol and PBS for 3 times, respectively (Cao et al., 2019). The cells were observed under a microscope and photographed (Leica, Germany). After oil red O staining, the lipid content was measured by isopropanol extraction of dye and optical density quantification (Wang et al., 2020). Absorbance was measured at 540 nm by using a microplate reader (Molecular devices, Shanghai, China).

2.6.5. Measurement of TC and FC levels

RAW264.7 cells were treated as described above. Cellular cholesterol content was measured according to the mouse total cholesterol ELISA kit and mouse free cholesterol ELISA kit (Keshun science and technology co., Shanghai, China). Briefly, after treatment of compound **2** (12.5, 25, and 50 μM) for 24 h, the cells were washed once with PBS and centrifuged at 3000 rpm/min for 10 min at room temperature. Then, according to the manufacturer's instructions, TC and FC were measured using a microplate reader.

3. Results and discussion

3.1. Structure elucidation

Pogocablanol A (**1**) was obtained in the form of colorless crystals. Its molecular formula was established to be $C_{15}H_{24}O_4$ by HR-ESI-MS (*m*/*z* 291.1574 $[M + Na]^+$, calcd 291.1572), corresponding to four degrees of unsaturation. The IR spectrum displayed characteristic absorptions for hydroxy and carbonyl functionalities (3445 and 1737 cm^{-1}). The ^1H NMR spectrum of compound **1** (Table 1) showed signals of three tertiary methyls (δ_H 1.19, 1.22, and 1.27), two exchangeable hydroxy protons (δ_H 3.12 and 3.81), and several aliphatic methylenes and methines between δ_H 1.44 and 2.25 ppm. The ^{13}C NMR and DEPT data (Table 2) revealed the presence of 15 carbons, including three methyls, six methylenes, one methine, four oxygenated quaternary carbons, and one carbonyl carbon. The above functionalities account for one out of the four degrees of unsaturation, and the remaining three degrees suggest compound **1** to be tricyclic. A comprehensive analysis of the 2D NMR spectra was conducted to establish the planar structure of compound **1**. The ^1H–^1H COSY correlations of H_2-3/H_2-4, as well as the HMBC correlations of OH-5 and H_3-15 with C-1, C-4, and C-5; of H_2-4 with C-1, C-2, and C-5; and of H_2-3 with C-2, C-4, and C-5, established the existence of a five-membered carbocycle (ring A) possessing a hydroxy and a methyl group substituted at C-5 and a carbonyl group at C-2 in compound **1** (Fig. 2). Additionally, the ^1H–^1H COSY correlations of H-7/H_2-12/H_2-11, combined with the HMBC correlations from H_3-13 and OH-10 to C-9, C-10, and C-11, from H_3-14 to C-7, C-8, and C-9, constructed the substructure of a six-membered carbocycle (ring B) with a hydroxy group at C-10 and two methyl groups attached to C-8 and C-10, respectively. Regarding the linkage of rings A and B, the ^1H–^1H COSY correlation of H_2-6/H-7, together with the HMBC correlations of H_2-6 with C-1, C-2, C-5, C-7, and C-8, revealed that rings A and B were connected by a methylene bridge (C-6). Finally, based on the molecular formula and the ^{13}C chemical shifts of C-1 (δ_C 88.9) and C-8 (δ_C 84.7), a 1-O-8 ether linkage was deduced to form an interesting 1-oxaspiro[4,4]nonane unit in compound **1**.

In the NOESY spectrum, cross peaks of H_3-13/H-7 and H_3-14/OH-10 revealed the spatial orientations of these protons in **1** (Fig. 3). However, it was difficult to elucidate the stereochemistry of the spiro carbon C-1 due to a lack of available NOESY data. Fortunately, a single crystal of compound **1** was obtained and successfully analyzed by X-ray diffraction using Cu Kα radiation (Fig. 4) with a Flack parameter of −0.14(13). Therefore, the absolute configuration of compound **1** was unambiguously determined to be 1*S*,5*R*,7*R*,8*S*,10*R*.

Pogocablanol B (**2**) appears as colorless crystals, with the same molecular formula, $C_{15}H_{24}O_4$, as compound **1**. Comparison of the ^1H, ^{13}C, and 2D NMR data of **2** and **1** (Tables 1 and 2 and Fig. 2) suggested that the two compounds have the same planar structure. Their ^{13}C NMR data showed minor differences in the same deuterated solvent. The C-7, C-9, C-10, C-11, C-12, and C-13 resonances in

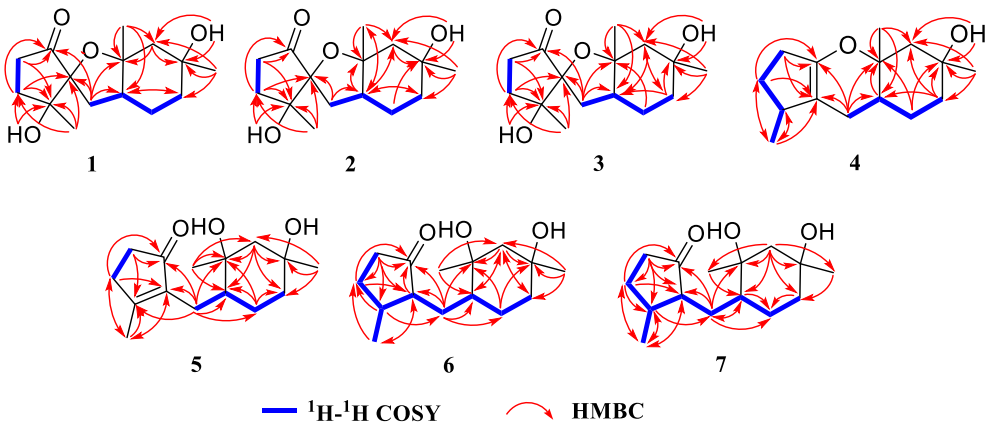

Fig. 2. Key ^1H–^1H COSY and HMBC correlations of **1**–**7**.

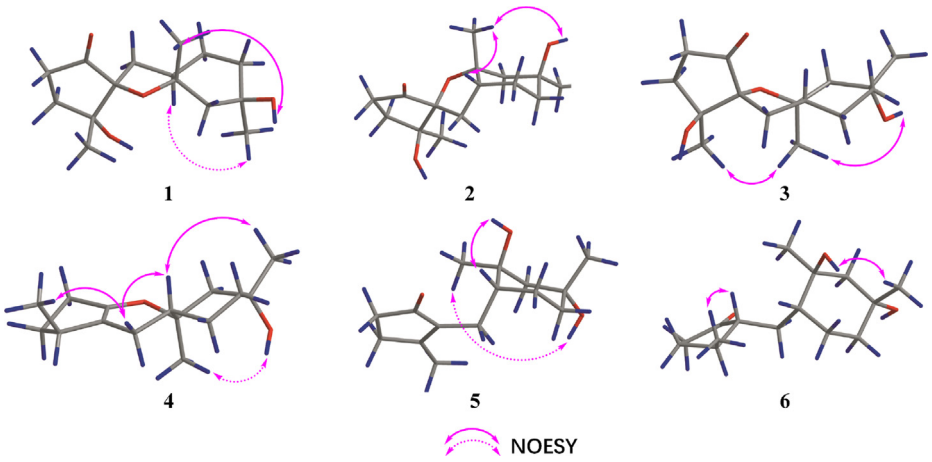

Fig. 3. Key NOESY correlations of **1**–**6.**

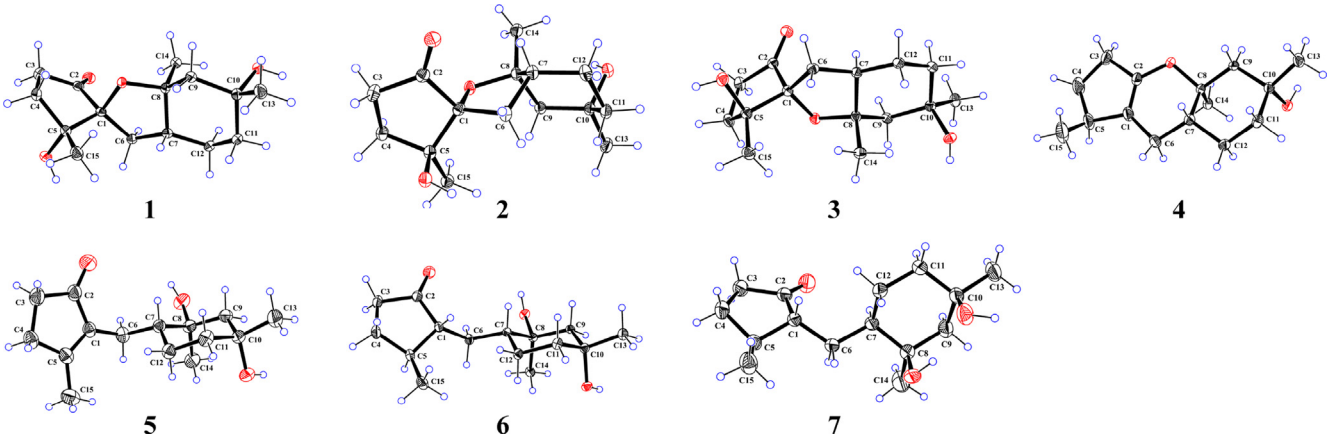

Fig. 4. X-ray crystallographic structures of **1**–**7**.

compound **2** were shielded by $\Delta\delta$ −7.3, −3.3, −1.5, −8.5, −2.0, and −1.1 ppm, respectively, while the C-6 and C-14 resonances in compound **2** were deshielded by $\Delta\delta$ +3.3 and +8.3 ppm, respectively. Therefore, compound **2** is a stereoisomer of compound **1**. The relative stereochemistry of H_3-14, H-7, and OH-10 in **2** was deduced from the NOESY data of H_3-14 with H-7 and OH-10 (Fig. 3). An X-ray diffraction experiment verified the planar structure of **2** and confirmed its absolute configuration to be 1*R*,5*S*,7*R*,8*R*,10*S* [Flack parameter = −0.01(12)] (Fig. 4).

Pogocablanol C (**3**) is an isomer of **1**, as indicated by HR-ESI-MS, ^{1}H NMR, and ^{13}C NMR data. Detailed analysis of the ^{1}H−^{1}H COSY, HSQC, and HMBC data confirmed that they have the same planar structure. The NOESY data and X-ray diffraction analysis [Flack parameter = 0.07(8)] further confirmed the structure and absolute configuration (1*R*,5*S*,7*R*,8*S*,10*R*) of compound **3**.

Pogocablanol D (**4**) was assigned a molecular formula of $C_{15}H_{24}O_2$ by an ion peak at *m*/*z* 259.1676 [M + Na]$^+$ in the HR-ESI-MS (calcd for $C_{15}H_{24}O_2Na$, 259.1674). The ^{1}H NMR data (Table 1) of compound **4** showed signals of three methyl groups, one exchangeable proton, and several aliphatic methylenes and methines. A total of 15 carbon signals, corresponding to three methyl groups, six methylenes, two methines, and four quaternary carbons (two olefinic), were revealed by its ^{13}C NMR (Table 2) and DEPT spectra. These data indicated that compound **4** was a pogocablane sesquiterpenoid similar to **3**. Ring A in **4** was confirmed by ^{1}H−^{1}H COSY correlations of H_2-3/H_2-4/H-5/H_3-15 and HMBC correlations of H_3-15 with C-1, C-4, and C-5; of H_2-3 with C-1 and C-5; and of H_2-4 with C-1, C-2, and C-15 (Fig. 2). Ring B in **4** was the same as that in **3**, as indicated by the ^{1}H−^{1}H COSY correlations of H_2-6/H-7/H_2-12/H_2-11, together with HMBC correlations from H_3-13 and OH-10 to C-9, C-10, and C-11; from H_3-14 to C-7, C-8, and C-9; and from H_2-12 to C-8 and C-10. Based on the HMBC correlations of H_2-6 with C-1, C-2, C-7, and C-8, the molecular formula, and the chemical shifts of C-2 (δ_C 149.7) and C-8 (δ_C 78.9), it was deduced that a pyran ring fused with rings A and B. A series of cross peaks of H_3-15/H-6a/H-7/H_3-13 and H_3-14/OH-10 observed in the NOESY spectrum of **4** revealed its relative stereochemistry (Fig. 3). A single crystal of **4** was obtained in MeOH for X-ray diffraction analysis [Flack parameter = 0.01(7)], which verified its absolute configuration to be 5*S*,7*R*,8*S*,10*R* (Fig. 4).

Pogocablanol E (**5**) has the molecular formula $C_{15}H_{24}O_3$ (HR-ESI-MS). The spectroscopic data of **5** resembled those of **4** (Tables 1 and 2), with the differences in the migration of the double bond from $\Delta^{1(2)}$ in **4** to $\Delta^{1(5)}$ in **5** and replacement of the oxygenated olefinic quaternary carbon (C-2) in **4** by a carbonyl (δ_C 209.1) in **5**. In addition, an extra exchangeable proton signal observed in the ^{1}H NMR spectrum of **5** suggested that a hydroxy group is attached to C-8 in **5** to match the molecular composition. Thus, rings A and B are connected only through a methylene group. The planar structure of **5** was further supported by ^{1}H−^{1}H COSY and HMBC data (Fig. 2), especially the ^{1}H−^{1}H COSY cross peaks of H_2-3/H_2-4 and H_2-6/H-7/H_2-12/H_2-11 and HMBC correlations from H_3-14

and OH-8 to C-7, C-8, and C-9; from H_2-12 to C-6, C-7, and C-8; from H_3-15 to C-1, C-4, and C-5; and from H_2-6 to C-1, C-2, C-5, C-7, C-8, and C-12. The NOESY correlations of H_3-14 with OH-10 and H-7 with OH-8 revealed the anti-orientation of OH-10 to H-7 and OH-8. Unambiguously, a single crystal of **5** was successfully analyzed by X-ray diffraction using Cu Kα radiation (Fig. 4) with a Flack parameter of –0.01(5). Therefore, the absolute configuration of **5** was determined as 7*R*,8*S*,10*R*.

Pogocablanol F (**6**) had similar NMR data to **5**. The molecular formula of compound **6** was determined as $C_{15}H_{26}O_3$ with two more hydrogen atoms than compound **5**. By comparing the ^1H and ^{13}C NMR data of **6** and **5**, the only difference between them was that the $\Delta^{1(5)}$ double bond in **5** was reduced in **6**. The planar that the $\Delta^{1(5)}$ double bond in **5** was reduced in **6**. The planar structure of **6** was confirmed by ^1H–^1H COSY and HMBC data analysis

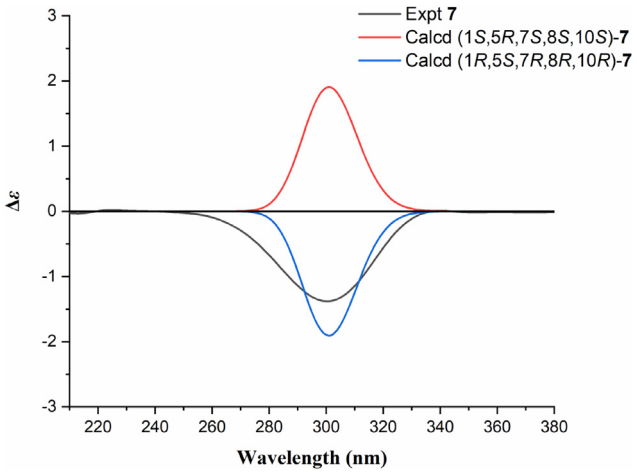

Fig. 5. The experimental and calculated ECD spectra of compound **7**.

(Fig. 2), especially the ^1H–^1H COSY correlations of H_2-3/H_2-4/H-5/H-1/H_2-6/H-7/H_2-12/H_2-11. In the NOESY spectrum, only two available correlations were observed (H_3-13/OH-8 and H_3-15/H-1). Fortunately, the X-ray diffraction data of compound **6** indicated that its absolute configuration is 1*R*,5*S*,7*R*,8*S*,10*R* [Flack parameter = –0.07(7)].

The IR, HR-ESI-MS, and NMR data of compound **7** indicated that it is an epimer of **6**. The X-ray diffraction data of **7** (Fig. 4) confirmed its relative configuration; however, its absolute configuration could not be confirmed reliably [Flack parameter = 0.13(10)]. Comparison of the experimental and calculated ECD data of **7** revealed its configuration as 1*R*,5*S*,7*R*,8*R*,10*R* (Fig. 5). Therefore, the structure of pogocablanol G (**7**) was defined as (1*R*,5*S*,7*R*,8*R*,10*R*)-pogocabla-8,10-diol-2-one.

The biogenetic origin of pogocablanols A–G (**1**–**7**) could plausibly be traced back to 5-epi-α-bulnesene (Scheme 1), a guaiane-type sesquiterpene that has been found in the essential oils of plants (Moronkola et al., 2015; Cai et al., 2014). First, the $\Delta^{1,10}$ bond of bulnesene is oxidatively cleaved to form intermediate **i**, which contains two characterized carbonyl units (Zhou et al., 2022). The Prins reaction is an acid-catalyzed condensation of alkenes with ketones or aldehydes, which is widely used in the fragrance industry (Doro et al., 2019). Due to the non-stereoselectivity, intermediate **i** is likely to undergo an intramolecular Prins reaction to construct two epimers (intermediates **ii** and **iii**) (Meinwald and Yankeelov, 1958; Doro et al., 2019). Then, intermediate **ii** is nucleophilically attacked by H_2O to form two sesquiterpenoids featuring a C5-C1-C6 skeleton system with three methyl groups (**6** and **7**). Subsequently, pogocablanol D (**4**) was generated through hemiketalation and dehydration from pogocablanol F (**6**) (Xiong et al., 2015). In addition, pogocablanol F (**6**) was oxidized to afford pogocablanol E (**5**). Successive oxidation, nucleophilic substitution, and etherification of **5** would afford pogocablanols A and C (**1** and **3**) substitution processes (Zhou et al., 2022). Pogocablanol B (**2**) could be yielded from intermediate **iii** through the same reaction processes used for the generation of pogocablanols A and C due

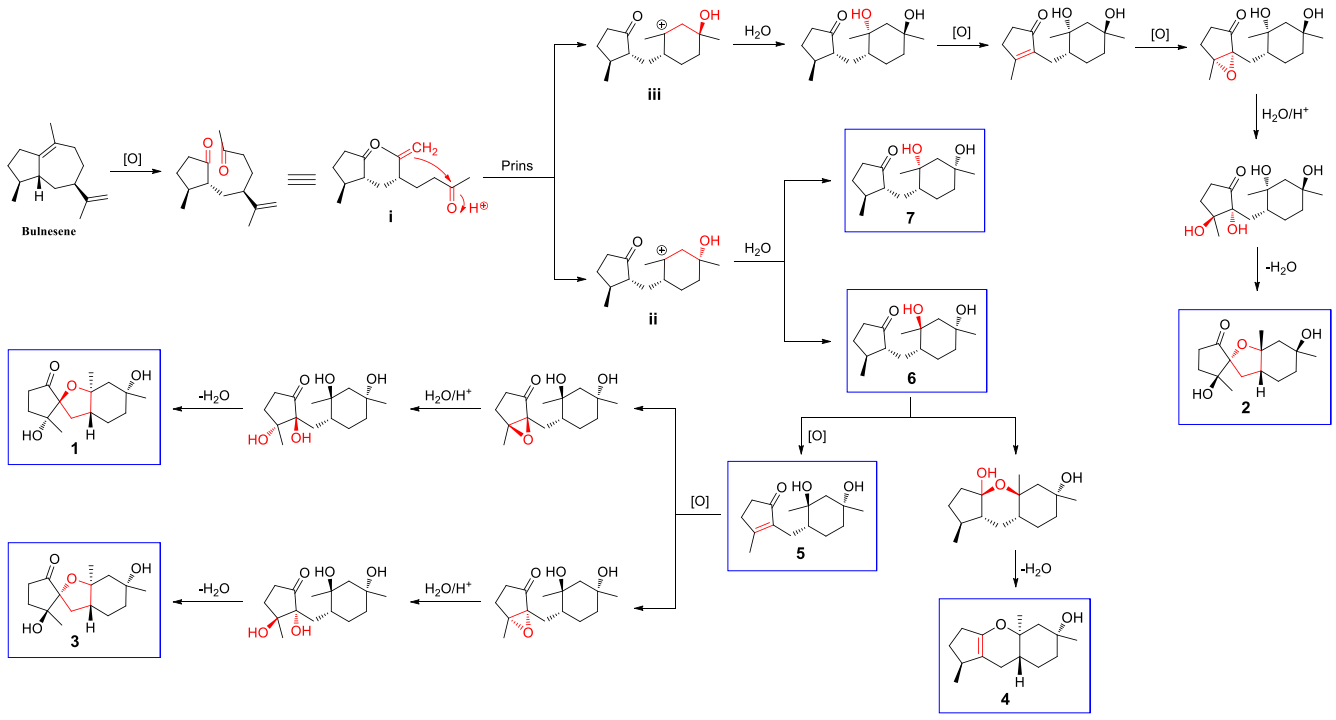

Scheme 1. Possible biosynthetic pathways for pogocablanols A–G (**1**–**7**).

to the stereoselectivity in the epoxidation and nucleophilic (**1** and **3**).

3.2. Biological activities

3.2.1. Relaxing effects on rat jejunum smooth muscle

The aerial part of *P. cablin* (patchouli) is used as a traditional Chinese medicine for the treatment of abdominal pain, vomiting, and diarrhea. It is well known that gastrointestinal smooth muscle spasms can cause abdominal pain and diarrhea, which occur frequently in the clinic. Modern studies have reported that patchouli and its compound preparations (Huoxiang Zhengqi Oral Liquid and Huoxiang Zhengqi Capsule) have good effects on intestinal disorders such as diarrhea-predominant irritable bowel syndrome, intestinal mucositis, acute colitis, and diarrhea (Chen et al., 2021; Guo et al., 2021; Gan et al., 2020; Yu et al., 2017), while patchouli and its extract act as relaxants on intestinal smooth muscles (Chen et al., 1998; Zhou et al., 2018b). Therefore, the regulatory effects of pogocablanols A–G on intestinal functions were investigated using an *in vitro* model of Ach-induced contraction of isolated rat jejuna. As shown in Fig. 6, compounds **1**–**4**, at concentrations of 0.5, 1.5, 5, 15, and 50 μM, significantly decreased the contraction tension of the rat jejuna smooth muscle induced by Ach compared to the control group ($P < 0.01$ or $P < 0.05$), compounds **5**–**7** had no significant effects. The E_{max} values of **1**, **2**, **3**, and **4** against Ach-induced contractions were 57.19 ± 10.17%, 69.02 ± 7.54%, 63.29 ± 14.42%, and 48.87 ± 4.01%, respectively. After comparing the results, the preliminary structure–activity relationships of these pogocablane-type sesquiterpenoids were obtained. The only difference between **1**–**4** and **5**–**7** was the linkage of the five- and six-membered carbocyclic rings (A and B). Thus, it can be inferred that the ether linkage between rings A and B to form an oxygen heterocycle plays an important role in the intestinal regulatory function. In addition, comparison of the effects of compounds **1**–**3** and **4** indicated that the 1-oxaspiro[4,4]nonane moiety is more beneficial for this relaxing effect than the pyran ring in pogocablanol-type sesquiterpenoids.

3.2.2. Inhibitory activity against ox-LDL-induced RAW264.7 macrophage foam cells formation

Structurally diverse sesquiterpenoids, such as pachouli alcohol, a major component of pachouli oil, have been reported to have inhibitory effects on atherosclerosis (Liu et al., 2015; He et al., 2021; Wang et al., 2016). To investigate the potential roles of these novel pogocablane-type compounds in atherosclerosis progression, Nile red staining, Oil red O staining, and a cholesterol assay were performed to evaluate the inhibitory activity against ox-LDL-induced foam cell formation. First, compounds **1**–**7** were tested for their cytotoxicity in RAW264.7 macrophages, and the results showed no cytotoxicity at concentrations of 12.5, 25, and 50 μM. Subsequently, adipogenesis was analyzed by Nile red staining in RAW264.7 macrophages after treatment with ox-LDL and different concentrations of compounds **1**–**7**. As shown in Fig. 7, at concentrations of 12.5, 25, and 50 μM, compound **2** significantly attenuated ox-LDL-induced adipogenesis in RAW264.7 macrophages in a concentration-dependent manner, while the other compounds showed no such activity.

Oil red O staining was further used to confirm the effect of compound **2** on lipid accumulation in RAW264.7 macrophages. As shown in Fig. 8A and 8B, there was a large amount of red staining, indicating more lipid accumulation in the model group than the control group. The addition of compound **2** to ox-LDL-induced foam cells significantly decreased the lipid accumulation. These results suggest that compound **2** could decrease intracellular lipid accumulation in ox-LDL-induced macrophages.

The levels of cellular total cholesterol (TC) and free cholesterol (FC) were determined by ELISA, and the level of cholesteryl ester (CE) was calculated as CE = TC − FC. Compared to the model group, the levels of TC, FC, and CE in RAW264.7 macrophages were significantly decreased by treatment with compound **2** (all $P < 0.01$)

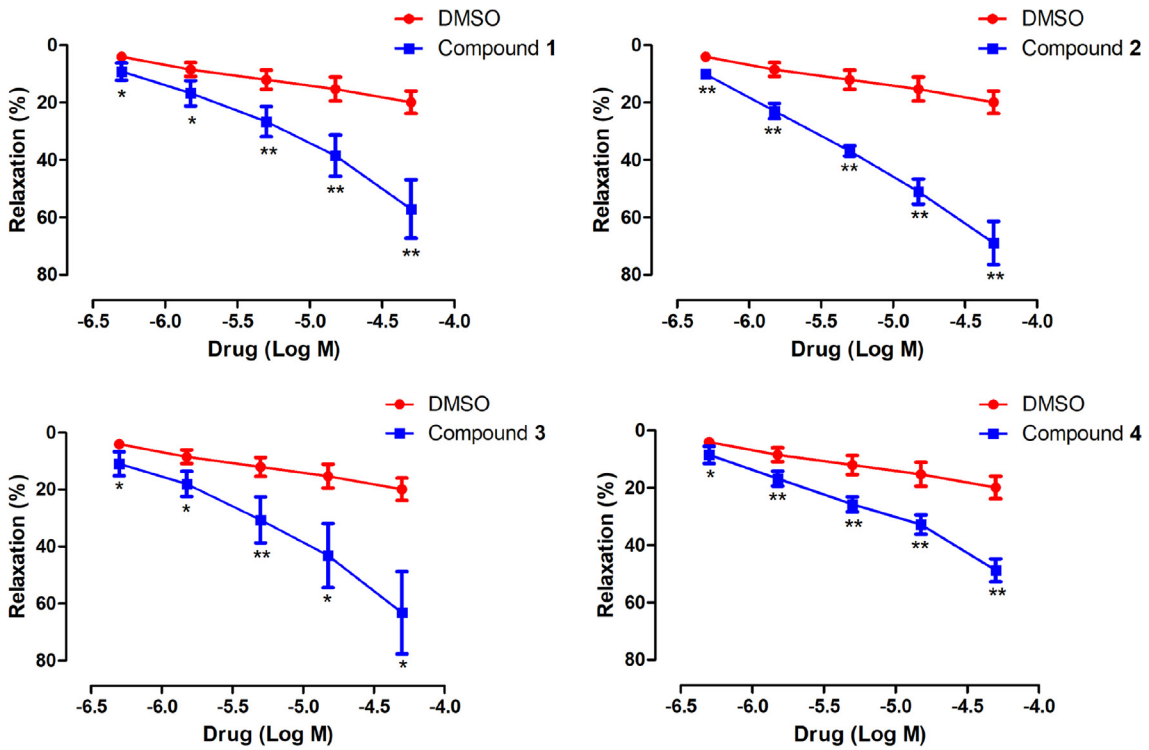

Fig. 6. Relaxing effects of compounds **1**, **2**, **3**, and **4** on isolated rat jejunum pre-contracted with Ach. Data are shown as the mean ± SD (n ≥ 3). *$P < 0.05$, **$P < 0.01$ vs. control group.

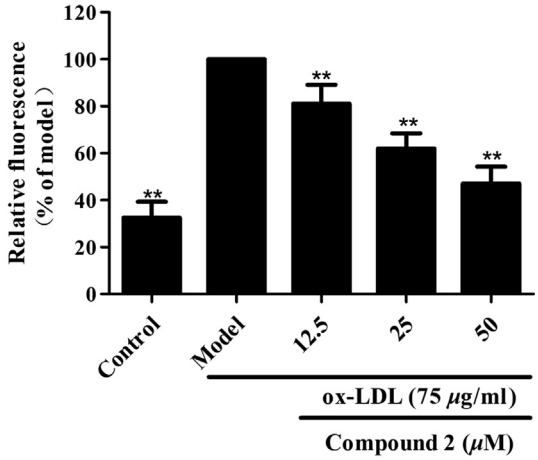

Fig. 7. Inhibitory activity of compound **2** against ox-LDL-induced adipogenesis in RAW264.7 macrophages. The lipid content was measured by Nile red staining. Data are shown as the mean ± SD (n = 3). $^{**}P < 0.01$ vs. model group.

(Fig. 8C–8E). These results suggest that compound **2** inhibits ox-LDL-induced lipid accumulation in macrophages.

4. Conclusions

In conclusion, we discovered an unprecedented bicyclic sesquiterpenoid skeleton with diverse structures (pogocablanols A–G) from the essential oil of *P. cablin*. This novel type of sesquiterpenoids was named the pogocablane type. Compounds **1**–**3** possess an interesting 1-oxaspiro[4,4]nonane moiety, while compound **4** has a pyran ring connecting the two carbocycles. Compounds **1**–**4** inhibited Ach-induced contraction of rat jejunum strips, with E_{max} values varying from 48.87 ± 4.01% to 69.02 ± 7.54%. Additionally, compound **2** displayed inhibitory activity against ox-LDL-induced RAW264.7 macrophage-derived foam cell formation. These findings expand our knowledge of the structural diversity of natural sesquiterpenoids, improve our understanding of the mechanisms underlying the traditional functions of patchouli, and provide ideas to boost the drug discovery for the treatment of gastrointestinal diseases.

Funding

This work was supported by the National Natural Science Foundation of China (NNSFC, Grant Nos. 81903779, 82022072, and 81891012), the Natural Science Foundation of Sichuan (Grant No. 2022NSFC1577), the Innovation Team Program of Jinan City (Grant No. 202228038), the Innovation Team and Talents Cultivation Program of the National Administration of Traditional Chinese Medicine (Grant No. ZYYCXTD-D-202209), the Scientific and Technological Industry Innovation Team of Traditional Chinese Medicine of Sichuan Province (Grant No.2022C001), and the "Xinglin Scholar" Plan of Chengdu University of Traditional Chinese Medicine (Grant Nos. XKTD2022006 and 030058064).

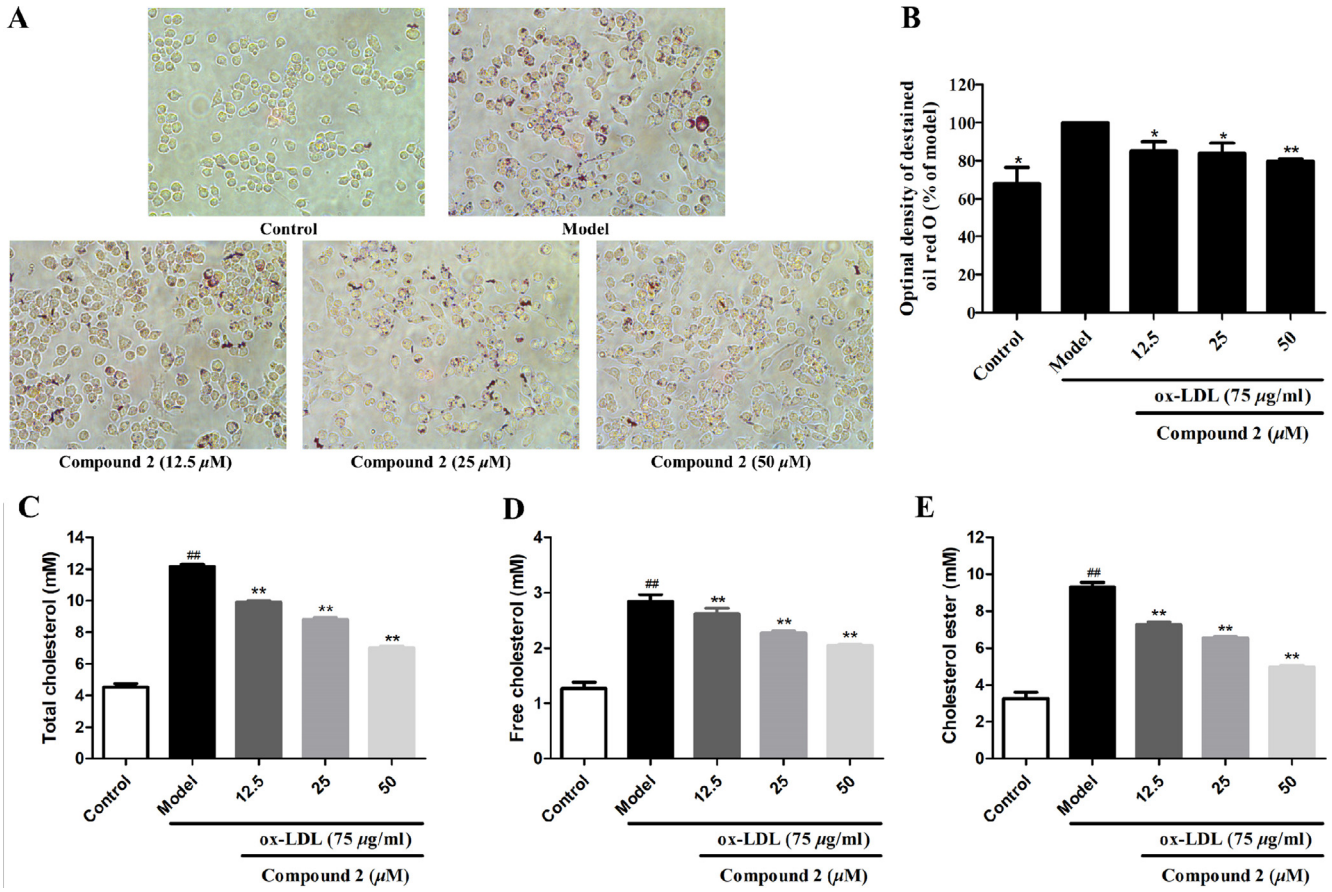

Fig. 8. Inhibitory activity of compound **2** against ox-LDL-induced lipid accumulation in foam macrophages, and cholesterol content in normal cells and foam cells. (A) The extent of lipid loading was assessed by Oil red O staining. The magnification of each panel is × 400. (B) Intracellular lipid deposition. (C) Content of total cholesterol (TC). (D) Content of free cholesterol (FC). (E) Content of cholesteryl ester (CE). Data are shown as the mean ± SD (n = 3). $^{*}P < 0.05$, $^{**}P < 0.01$ vs. model group.

Declaration of Competing Interest

The authors declare that they have no known competing financial interests or personal relationships that could have appeared to influence the work reported in this paper.

Appendix A. Supplementary data

Supplementary data to this article can be found online at https://doi.org/10.1016/j.arabjc.2023.105245.

References

Bian, X., Zhou, R., Yang, Y., Li, P., Hang, Y., Hu, Y., Yang, L., Wen, D., 2015. Divergent effect of dezocine, morphine and sufentanil on intestinal motor function in rats. Int. J. Med. Sci. 12, 848–852. https://doi.org/10.7150/ijms.12616.

Cai, J., Lin, C., Lin, G., Xiang, Z., 2014. Chemical constituents analysis of volatile oils from different parts of Alpinia Japonica Miq. in Wenzhou by GC–MS. Chin. Arch. Trad. Chin. Med. 32, 893–896. https://doi.org/10.13193/j.issn.1673-7717.2014.04.064.

Cao, H., Jia, Q., Yan, L., Chen, C., Xing, S., Shen, D., 2019. Quercetin suppresses the progression of atherosclerosis by regulating MST1-mediated autophagy in ox-LDL-induced RAW264.7 macrophage foam cells. Int. J. Mol. Sci. 20, 6093. https://doi.org/10.3390/ijms20236093.

Chen, X., He, B., Li, X., Li, H., Luo, J., 1998. Comparison of effects of three extrats of herba pogostemonis on the intestinal function. Pharmacol. Clin. Chin. Mater. Med. 14, 32–34. https://doi.org/10.13412/j.cnki.zyyl.1998.02.016.

Chen, Q.F., Liu, Z.P., Wang, F.P., 2011. Natural sesquiterpenoids as cyto-toxic anticancer agents. Mini Rev. Med. Chem. 11, 1153–1164. https://doi.org/10.2174/138955711797655399.

Chen, J., Xie, X., Li, M., Xiong, Q., Li, G., Zhang, H., Chen, G., Xu, X., Yin, Y., Peng, F., Peng, C., 2021. Pharmacological activities and mechanisms of action of *Pogostemon cablin* Benth: a review. Chin. Med. 16, 5. https://doi.org/10.1186/s13020-020-00413-y.

Chen, M., Zhang, J., Lai, Y., Wang, S., Li, P., Xiao, J., Fu, C., Hu, H., Wang, Y., 2013. Analysis of *Pogostemon cablin* from pharmaceutical research to market performances. Expert Opin. Invest. Drugs 22, 245–257. https://doi.org/10.1517/13543784.2013.754882.

Chen, Y., Zhao, J., Li, S., Xu, J., 2019. Total synthesis of sesterterpenoids. Nat. Prod. Rep. 36, 263–288. https://doi.org/10.1039/c8np00050f.

Doro, F., Akeroyd, N., Schiet, F., Narula, A., 2019. The prins reaction in the fragrance industry: 100th anniversary (1919–2019). Angew. Chem. Int. Ed. 58, 7174–7179. https://doi.org/10.1002/anie.201814470.

Frage, B.M., 2013. Natural sesquiterpenoids. Nat. Prod. Rep. 30, 1226–1264. https://doi.org/10.1039/c3np70047j.

Galovičová, L., Borotová, P., Valková, V., Ďúranová, H., Štefániková, J., Vukovic, N.L., Vukic, M., Kačániová, M., 2022. Biological activity of *Pogostemon cablin* essential oil and its potential use for food preservation. Agronomy 12, 387. https://doi.org/10.3390/agronomy12020387.

Gan, Y., Ai, G., Wu, J., Luo, H., Chen, L., Huang, Q., Wu, X., Xu, N., Li, M., Su, Z., Liu, Y., Huang, X., 2020. Patchouli oil ameliorates 5-fluorouracil-induced intestinal mucositis in rats via protecting intestinal barrier and regulating water transport. J. Ethnopharmacol. 250,. https://doi.org/10.1016/j.jep.2019.112519 112519.

García-Davis, S., Sifaoui, I., Reyes-Batlle, M., Viveros-Valdez, E., Piñero, J.E., Lorenzo-Morales, J., Fernández, J.J., Díaz-Marrero, A.R., 2018. Anti-*acanthamoeba* activity of brominated sesquiterpenes from *Laurencia johnstonii*. Mar. Drug. 16, 443. https://doi.org/10.3390/md16110443.

Ghayur, M.N., Gilani, A.H., Houghton, P.J., 2005. Species differences in the gut stimulatory effects of radish seeds. J. Pharm. Pharmacol. 57, 1493–1501. https://doi.org/10.1211/jpp.57.11.0016.

Guo, X., Xuan, M., Zheng, H., Qin, S., Wu, H., Huang, S., Wen, Z., 2021. The Chinese herbal formula Huoxiang Zhengqi for diarrhea-predominant irritable bowel syndrome (CHAIRS): a study protocol for a double-blinded randomized controlled trial. Trials 22, 491. https://doi.org/10.1186/s13063-021-05444-w.

He, L., Weng, H., Li, Q., Shi, G., Liu, X., Du, Y., Zheng, J., Ling, W., Wang, D., 2021. Wang, Lactucopicrin inhibits cytoplasmic dynein-mediated NF-κB activation in inflammated macrophages and alleviates atherogenesis in apolipoprotein E-deficient mice. Mol. Nutr. Food Res. 65, 2000989. https://doi.org/10.1002/mnfr.202000989.

Hu, G.Y., Peng, C., Xie, X.F., Xiong, L., Zhang, S.Y., Cao, X.Y., 2018. Patchouli alcohol isolated from Pogostemon cablin mediates endothelium independent vasorelaxation by blockade of Ca2+ channels in rat isolated thoracic aorta. J. Ethnopharmacol. 220, 188–196. https://doi.org/10.1016/j.jep.2017.09.036.

Jiang, S., Wang, M., Jiang, Z., Zafar, S., Xie, Q., Yang, Y., Liu, Y., Yuan, H., Jian, Y., Wang, W., 2021. Chemistry and pharmacological activity of sesquiterpenoids from the Chrysanthemum genus. Molecules 26, 3038. https://doi.org/10.3390/molecules26103038.

Liu, Y., Liu, W., Peng, Q.X., Peng, J.L., Yu, L.Z., Hu, J.L., 2014. Protective effect of Huoxiang Zhengqi Oral Liquid on intestinal mucosal mechanical barrier of rats with postinfectious irritable bowel syndrome induced by acetic acid. Evid. Based Complement. Alternat. Med. 2014,. https://doi.org/10.1155/2014/218383 218383.

Liu, M., Mao, L., Daoud, A., Hassan, W., Zhou, L., Lin, J., Liu, J., Shang, J., 2015. β-elemene inhibits monocyte-endothelial cells interactions via reactive oxygen species/MAPK/NF-κB signaling pathway in vitro. Eur. J. Pharmacol. 766, 37–45. https://doi.org/10.1016/j.ejphar.2015.09.032.

Meinwald, J., Yankeelov, J.A., 1958. The synthesis and acid-catalyzed cyclization of α-methylheptenone. J. Am. Chem. Soc. 80, 5266–5270. https://doi.org/10.1021/ja01552a062.

Moronkola, D.O., Yeboah, S.O., Majinda, R.R.T., Sichilongo, K., 2015. Compositions of *Harungana madagascariensis* Lam. ex Poiret leaf and stem essential oils. J. Chem. Pharm. Res. 7, 959–964.

Swamy, M.K., Sinniah, U.R., 2015. A comprehensive review on the phytochemical constituents and pharmacological activities of *Pogostemon cablin* Benth.: An aromatic medicinal plant of industrial importance. Molecules 20, 8521–8547. https://doi.org/10.3390/molecules20058521.

Tao, Q., Ma, K., Yang, Y., Wang, K., Chen, B., Huang, Y., Han, J., Bao, L., Liu, X.B., Yang, Z., Yin, W.B., Liu, H., 2016. Bioactive sesquiterpenes from the edible mushroom Flammulina velutipes and their biosyn-thetic pathway confirmed by genome analysis and chemical evidence. J. Org. Chem. 81, 9867–9877. https://doi.org/10.1021/acs.joc.6b01971.

Wang, Y., Bao, L., Yang, X., Li, L., Li, S., Gao, H., Yao, X.S., Wen, H., Liu, H.W., 2012. Bioactive sesquiterpenoids from the solid culture of the edible mushroom Flammulina velutipes growing on cooked rice. Food Chem. 132, 1346–1353. https://doi.org/10.1016/j.foodchem.2011.11.117.

Wang, Y., Li, Z., Liu, B., Wu, R., Gong, H., Su, Z., Zhang, S., 2020. Isoborneol attenuates low-density lipoprotein accumulation and foam cell formation in macrophages. Drug Des. Devel. Ther. 14, 167–173. https://doi.org/10.2147/DDDT.S233013.

Wang, H.T., Wang, Z.Z., Wang, Z.C., Wang, S.M., Cai, X.J., Su, G.H., Yuan, Z.Y., 2016. Patchouli alcohol attenuates experimental atherosclerosis via inhibiting macrophage infiltration and its inflammatory responses. Biomed. Pharmacother. 83, 930–935. https://doi.org/10.1016/j.biopha.2016.08.005.

Xiong, L., Zhou, Q.M., Zou, Y., Chen, M.H., Guo, L., Hu, G.Y., Liu, Z.H., Peng, C., 2015. Leonuketal, a spiroketal diterpenoid from *Leonurus japonicus*. Org. Lett. 17, 6238–6241. https://doi.org/10.1021/acs.orglett.5b03227.

Xu, F., Cai, W., Ma, T., Zeng, H., Kuang, X., Chen, W., Liu, B., 2022. Traditional uses, phytochemistry, pharmacology, quality control, industrial application, pharmacokinetics and network pharmacology of *Pogostemon cablin*: a comprehensive review. Am. J. Chin. Med. 55, 691–721. https://doi.org/10.1142/S0192415X22500288.

Yu, X., Yang, G., Jiang, H., Lin, S., Liu, Y., Zhang, X., Zeng, H., Su, Z., Huang, S., Shen, L., Zhang, X., 2017. Patchouli oil ameliorates acute colitis: A targeted metabolite analysis of 2,4,6-trinitrobenzenesulfonic acid-induced rats. Experiment. Ther. Med. 14, 1184–1192. https://doi.org/10.3892/etm.2017.4577.

Yuan, L., Li, Q., Zhang, Z., Liu, Q., Wang, X., Fan, L., 2020. Tanshinone IIA inhibits the adipogenesis and inflammatory response in ox-LDL-challenged human monocyte-derived macrophages via regulating miR-130b/WNT5A. J. Cell. Biochem. 121, 1400–1408. https://doi.org/10.1002/jcb.29375.

Zhao, M., Chen, Y., Wang, C., Xiao, W., Chen, S., Zhang, S., Yang, L., Li, Y., 2019. Systems pharmacology dissection of multi-scale mechanisms of action of Huo-Xiang-Zheng-Qi Formula for the treatment of gastrointestinal diseases. Front. Pharmacol. 9, 1448. https://doi.org/10.3389/fphar.2018.01448.

Zhou, Q.M., Chen, M.H., Li, X.H., Peng, C., Lin, D.S., Li, X.N., He, Y., Xiong, L., 2018a. Absolute configurations and bioactivities of guaiane-type sesquiterpenoids isolated from *Pogostemon cablin*. J. Nat. Prod. 81, 1919–1927. https://doi.org/10.1021/acs.jnatprod.7b00690.

Zhou, T.R., Huang, J.J., Huang, Z.T., Cao, H.Y., Tan, B., 2018b. Inhibitory effects of patchouli alcohol on stress-induced diarrhea-predominant irritable bowel syndrome. World J. Gastroenterol. 24, 693–705. https://doi.org/10.3748/wjg.v24.i6.693.

Zhou, Q.M., Zhao, H.Y., Ma, C., Huang, L., Liu, J., Guo, L., Peng, C., Xiong, L., 2022. Pocahemiketone A, a sesquiterpenoid possessing a spirocyclic skeleton with a hemiketal endoperoxide unit, alleviates $A\beta_{25-35}$-induced pyroptosis and oxidative stress in SH-SY5Y cells. Org. Lett. 24, 4734–4738. https://doi.org/10.1021/acs.orglett.2c01587.

Zhu, H., Zhou, Q.M., Peng, C., Chen, M.H., Li, X.N., Lin, D.S., Xiong, L., 2017. Pocahemiketals A and B, two new hemiketals with unprecedented sesquiterpenoid skeletons from *Pogostemon cablin*. Fitoterapia 120, 67–71. https://doi.org/10.1016/j.fitote.2017.05.013.